



HAL
open science

Quantum state-resolved gas/surface reaction dynamics probed by reflection absorption infrared spectroscopy

Li Chen, Hirokazu Ueta, Régis Bisson, Rainer D. Beck

► **To cite this version:**

Li Chen, Hirokazu Ueta, Régis Bisson, Rainer D. Beck. Quantum state-resolved gas/surface reaction dynamics probed by reflection absorption infrared spectroscopy. *Review of Scientific Instruments*, 2013, 84, pp.053902. 10.1063/1.4803933 . hal-00833941

HAL Id: hal-00833941

<https://hal.science/hal-00833941>

Submitted on 18 Nov 2015

HAL is a multi-disciplinary open access archive for the deposit and dissemination of scientific research documents, whether they are published or not. The documents may come from teaching and research institutions in France or abroad, or from public or private research centers.

L'archive ouverte pluridisciplinaire **HAL**, est destinée au dépôt et à la diffusion de documents scientifiques de niveau recherche, publiés ou non, émanant des établissements d'enseignement et de recherche français ou étrangers, des laboratoires publics ou privés.

Quantum state-resolved gas/surface reaction dynamics probed by reflection absorption infrared spectroscopy

Li Chen,¹ Hirokazu Ueta,² Régis Bisson,³ and Rainer D. Beck^{2,a)}

¹Department of Dynamics at Surfaces, Max Planck Institute for Biophysical Chemistry, Am Faßberg 11, Göttingen, Germany

²Laboratoire de Chimie Physique Moléculaire, Ecole Polytechnique Fédérale de Lausanne, Switzerland

³Aix-Marseille Université, PIIM, CNRS, UMR 7345, 13397 Marseille, France

(Received 22 February 2013; accepted 22 April 2013; published online 9 May 2013)

We report the design and characterization of a new molecular-beam/surface-science apparatus for quantum state-resolved studies of gas/surface reaction dynamics combining optical state-specific reactant preparation in a molecular beam by rapid adiabatic passage with detection of surface-bound reaction products by reflection absorption infrared spectroscopy (RAIRS). RAIRS is a non-invasive infrared spectroscopic detection technique that enables online monitoring of the buildup of reaction products on the target surface during reactant deposition by a molecular beam. The product uptake rate obtained by calibrated RAIRS detection yields the coverage dependent state-resolved reaction probability $S(\theta)$. Furthermore, the infrared absorption spectra of the adsorbed products obtained by the RAIRS technique provide structural information, which help to identify nascent reaction products, investigate reaction pathways, and determine branching ratios for different pathways of a chemisorption reaction. Measurements of the dissociative chemisorption of methane on Pt(111) with this new apparatus are presented to illustrate the utility of RAIRS detection for highly detailed studies of chemical reactions at the gas/surface interface. © 2013 AIP Publishing LLC. [<http://dx.doi.org/10.1063/1.4803933>]

I. INTRODUCTION

Detailed experimental studies of gas/surface reaction dynamics are essential for the development of a predictive understanding of chemical reactions occurring at the gas/surface interface including heterogeneous catalysis.¹ The emergence of quantum state-resolved experimental techniques using state-specific reactant preparation by laser excitation of the incident species has greatly increased the level of detail available from molecular beam experiments.^{2–4} State-resolved reactivity measurements have demonstrated both mode-specificity and bond-selectivity^{5–9} as well as stereodynamical control¹⁰ for chemisorption of methane on transition metal surfaces. Highly detailed data provided by state-resolved experiments enable stringent tests of *ab initio* theory of gas/surface reaction dynamics,^{11,12} helping experimentalists and theorists to work towards the ultimate goal of using computers to predict surface reactivity with chemical accuracy in order to design and optimize heterogeneous catalysts.

For state-resolved reactivity measurements, a significant fraction of the gas-phase reactant species is excited to a specific rovibrational quantum state using infrared¹³ or Raman¹⁴ pumping in a molecular beam incident on the reactive surface (laser-on conditions). Any surface bound reaction products formed as a result of the gas/surface collisions are detected quantitatively by surface analytical methods such as Auger electron spectroscopy (AES),^{15,16} secondary ion mass spectrometry (SIMS),¹⁷ or temperature programmed reac-

tion techniques (TPR).⁸ Comparison with identical deposition conditions but without IR pumping (laser-off conditions) is used to reveal the effect of rovibrational excitation on the reactivity and yields the state-resolved reactivity from the difference between the laser-on and laser-off measurements.¹³ One of the drawbacks of the products detection methods applied in previous state-resolved reactivity measurements is the invasive (AES) or even destructive nature (SIMS, TPR) of the detection process. As a consequence, quantification of the reaction products has to be performed *a posteriori*, following their accumulation over a predetermined deposition time. The recording of a full uptake curve, which relates the product coverage to the incident reactant dose, has to be done point-by-point by repeating the deposition experiment many times for different molecular beam exposures. With our AES detection a typical cleaning/deposition/analysis cycle for a methane reactivity measurement takes 2–3 h. Recording an uptake curve for one specific set of conditions (incident translation energy E_t , expansion nozzle temperature T_n , surface temperature T_s), therefore, takes at least a week. To make the state-resolved reactivity measurements feasible, the initial reaction probability was determined by performing a few depositions leading to less than 10% of the saturation coverage combined with the assumption that for low coverage the uptake curve can be approximated by a linear function.

Product detection by reflection absorption infrared spectroscopy (RAIRS), however, does not suffer from this drawback since the weak thermal infrared radiation emitted by the IR source of the Fourier transform infrared spectrometer (FTIR) affects neither the incident reactant molecules in the molecular beam nor can it lead to desorption or dissociation

^{a)}Author to whom correspondence should be addressed. Electronic mail: rainer.beck@epfl.ch

of the chemisorbed reaction products on the target surface. Therefore, RAIRS can be applied during the molecular beam exposure of the target surface to record the complete product uptake curve in a single deposition experiment. Differentiation of the uptake curve with respect to incident dose yields the coverage dependent reaction probability $S(\theta)$ including the initial reaction probability $S_0 = S(\theta = 0)$ from the initial slope at zero coverage as well as valuable information about the gas/surface reaction mechanism via the coverage dependent $S(\theta)$. The fact that deposition and data acquisition can be performed simultaneously rather than sequentially contributes to the higher signal/noise ratio for the RAIRS detection compared to AES, SIMS, or TPR.

Another important advantage of RAIRS stems from the fact that it is a surface vibrational spectroscopy technique^{18–20} which provides direct structural information through the characteristic vibrational frequencies of the absorbed species, allowing identification of the nascent products and the study of reaction pathways. Finally, RAIRS is applicable to a wide range of adsorbates as long as they possess at least one vibrational mode with a transition dipole moment component along the surface normal.

In this article, we describe the application of RAIRS as a detection method for quantum state-resolved studies of chemical reaction dynamics at surfaces. The material is organized as follows. First, we give an overview of the design of our experimental apparatus including the continuous molecular beam source, molecular beam characterization, and the surface analysis facilities in the UHV chamber. Then, we describe in detail the two essential features of this new machine: *rovibrational state selective* preparation of gas-phase reactants in the cw molecular beam by infrared optical pumping using rapid adiabatic passage (RAP) and *in situ* detection of the surface-bound reaction products by RAIRS. Finally, we present the first application of this setup to the dissociative chemisorption of methane isotopologues on Pt(111).

II. EXPERIMENTAL SETUP

A. Overview

Figure 1 shows a three-dimensional model of our molecular-beam/surface-science apparatus interfaced to an evacuated Bruker Vertex V70 FTIR spectrometer. The FTIR spectrometer and external infrared detector housing are connected to the UHV surface science chamber via flexible bellows to allow evacuation of the complete optical beam path of the FTIR setup to avoid contributions in the RAIRS signal from atmospheric absorptions of H_2O and CO_2 . The bellows can be removed for bakeout of the UHV chamber, which is needed to achieve the base pressure of 3×10^{-11} mbar.

Figure 2 shows details of the molecular beam path inside the machine. The vacuum system consists of a triply differentially pumped molecular beam source connected to a UHV surface science chamber. In the source chamber, pumped by a 2000 L/s wide range turbomolecular pump, a supersonic expansion is produced by expanding gas mixtures containing the reactant molecules with 1–10 bars stagnation pressure through a 50 μm diameter nozzle (made of Inconel 600) into

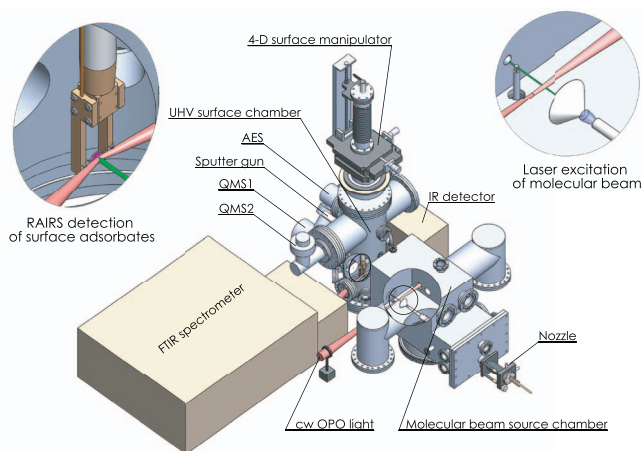


FIG. 1. Overview of the molecular-beam/surface-science UHV apparatus with FTIR spectrometer and external infrared detector for RAIRS detection.

the first differential pumping stage vacuum (10^{-8} mbar base pressure, 10^{-3} mbar with the molecular beam on). The nozzle is made from two concentric tubes that are closed at one end by a thin plate with the nozzle orifice laser drilled into its center.²¹ The nozzle can be heated to 800 °C by resistive heating using a DC current passing through the nozzle tubes. The nozzle temperature is measured by a *K*-type thermocouple, spot-welded to the outside of the nozzle tip, and is controlled by regulating the heating current of up to 60 A with a PID controller connected to the DC current supply.

The molecular beam path with the relevant dimensions is shown in Figure 3. A 1 mm diameter electroformed nickel skimmer (Beam Dynamics – model 2) located 15 to 65 mm from the nozzle is used to generate a molecular beam in the second differential pumping stage. The second stage, pumped by a 500 L/s turbo pump, includes a variable frequency chopper wheel with two 2 mm wide slits driven by a DC motor equipped with a position encoder that regulates the motor rotation speed in the range from 1 to 250 Hz with an accuracy of 0.1%. The chopper wheel is used in combination with an on-axis quadrupole mass spectrometer (QMS) to measure the speed distribution of the molecular beam by the time-of-

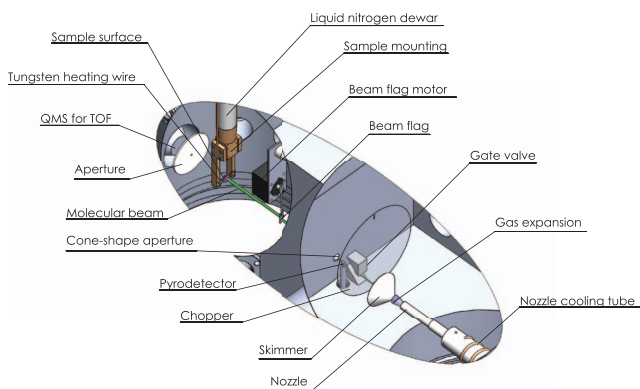


FIG. 2. Schematic of the molecular beam path including the supersonic expansion nozzle, molecular beam skimmer, chopper disk, pyroelectric detector, beam flag for King & Wells measurements, and the single crystal target surface mounted on a surface science manipulator.

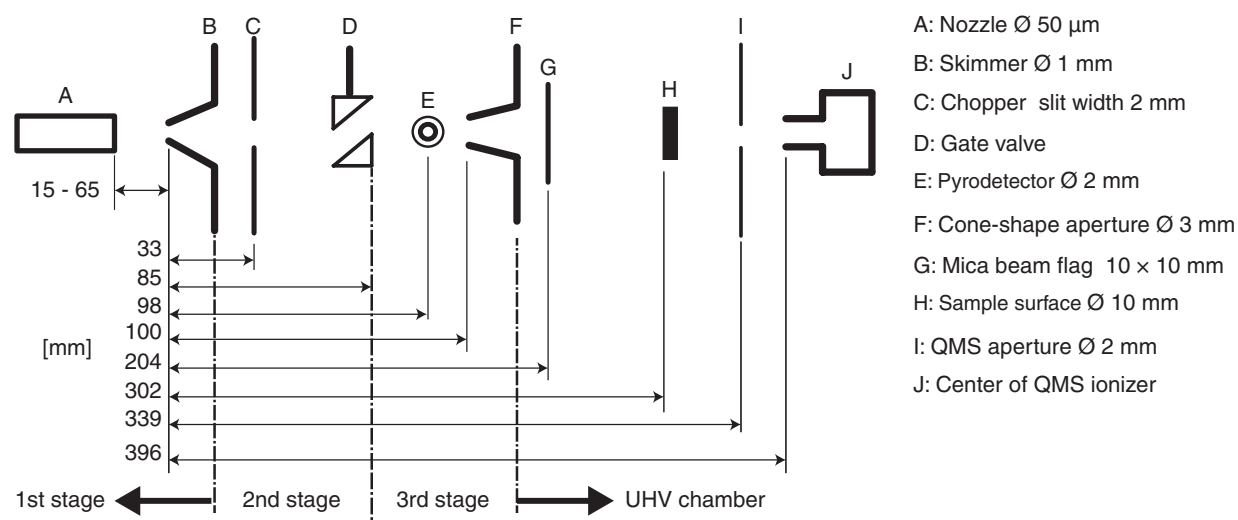


FIG. 3. Relevant dimensions (mm) in the molecular beam path.

flight method (TOF). The position encoder with a resolution of 2048 steps/rotation also makes it possible to precisely stop the chopper wheel in the “open position” so that the molecular beam passes through the center of one of the 2 mm wide slits cut into the circumference of the chopper wheel in order to generate a cw molecular beam used for the deposition experiments.

The second and third differential pumping stages are separated by a manually operated gate valve which allows for venting of the first and second vacuum stage of the molecular beam source while keeping the third and fourth stage under UHV conditions. The third differential pumping stage, pumped by a 500 L/s turbo pump, contains a pyroelectric detector mounted on a translation feedthrough so that it can be inserted in the molecular beam to detect either the kinetic energy or vibrational excitation of the molecular beam. Since this detector is only sensitive to changes in the temperature of its 2 mm diameter pyroelectric element, it can be used to detect either the translational energy of the molecular beam by spinning the chopper wheel to modulate the molecular beam or the vibrational excitation of the cw molecular beam by modulating the excitation laser intensity with an electromechanical shutter.

The molecular beam passes from the third differential pumping stage into the UHV surface science chamber through a 3 mm diameter skimmer aperture, designed to transmit a well collimated molecular beam into the UHV chamber while minimizing scattering or deflection of molecules out of the beam but into the UHV chamber. A simple round aperture used previously in this position was found to deflect a fraction of the molecular beam such that the molecules entered the UHV chamber but did not directly collide with the Pt(111) sample causing erroneously low King and Wells (K&W) reaction probability measurements (see below).^{22,23}

The collimated molecular beam enters the UHV chamber and collides with a 10 mm diameter sample surface with a typical beam spot size 7–8 mm in diameter, depending on the nozzle to skimmer distance.

The UHV chamber is equipped with several surface science techniques for surface preparation, characterization, and reaction probability measurements. A mica beam flag (10 \times 10 mm) can be used to block the molecular beam in front of the sample surface by a UHV compatible stepper-motor for K&W reaction probability measurements.²² A QMS is mounted on the molecular beam axis for measurements of the beam velocity distribution by the TOF method in combination with the chopper wheel mounted in the second differential pumping stage. A second QMS (Pfeiffer) with a UHV grid ion source in an off-axis position is used for temperature programmed desorption (TPD) measurements and for residual gas analysis (RGA) of the UHV background. An ion gun (Omicron, ISE100) serves for surface cleaning by Ar⁺ sputtering. The chemical composition of the target surface can be analyzed by AES with a PHI-155 cylindrical optical mirror analyzer.

The 10 mm diameter Pt(111) single crystal surface is held between two pre-shaped 0.38 mm thick W wires that are clamped on either end to a copper arm of the home built sample holder (Figure 4) following a design published by Yates.²⁴ The hollow central part of the sample holder is made of oxygen free high conductivity copper which is silver soldered to a vertical stainless steel cryotube of 126 cm length and which can be filled with liquid N₂ for sample cooling. Two copper arms are attached to the central part with sapphire spacers (Swiss Jewel, 15.5 mm diameter, and 0.5 mm thick). The sapphire spacers ensure that the copper arms are electrically isolated from the manipulator for sample heating by a DC current but in good thermal contact with the liquid N₂ reservoir for efficient sample cooling. The sample temperature is measured by a K-type thermocouple inserted in a 0.5 mm diameter hole cut into the side of the Pt(111) single crystal sample. Sample heating is achieved by heating the two W filaments with a DC current supplied by a regulated current supply. A PID temperature controller is used to stabilize the sample temperature to 0.1 K and to perform linear temperature ramps for TPD measurements.

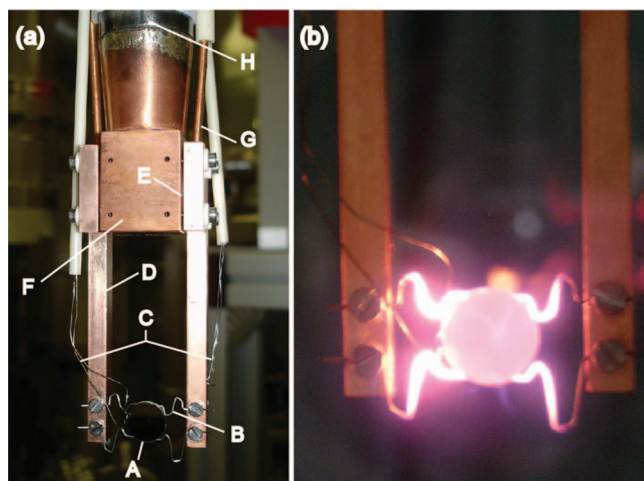


FIG. 4. (a) Photographs of the sample holder: (A) Pt(111) single crystal; (B) tungsten heating wires; (C) K-type thermocouples monitor the sample and the holder temperature; (D) copper arm are attached with sapphire spacers (E) to the central dewar assembly (F) filled with liquid nitrogen; (G) heating wire; (H) stainless steel liquid nitrogen cryotube; (b) Pt (111) sample heated to $T_s = 1000$ K.

A second thermocouple is attached to one of the copper arms in order to monitor the holder temperature during sample heating and cooling. The design of the sample mount ensures localized heating of the sample without raising the temperature of other parts of the manipulator (except for the heating filaments), which is important for TPD measurements.

The Pt(111) sample can be cooled from 300 K to 87 K in 10 min and heated from 87 K to 1200 K within 3 min (while the copper holder temperature increases less than 10 K) using 22 A of DC current. Sample temperatures as low as 70 K can be achieved by pumping on the liquid N_2 reservoir or by bubbling He gas through the liquid nitrogen for cooling by Helium transpiration.²⁴

B. Rovibrational state selective optical pumping using rapid adiabatic passage

Quantum state-specific reactant preparation is performed in the incident molecular beam using infrared light from a tunable, single mode, continuous-wave optical parametric oscillator (OPO, Argos Model 2400-SF, Model C, Lockheed Martin Acculight Corp.). The OPO idler output is tunable in the range of $3125\text{--}2560\text{ cm}^{-1}$ ($3.2\text{--}3.9\text{ }\mu\text{m}$) with an output power in excess of 1 W. To keep the OPO idler output resonant with the ro-vibrational transition used for reactant preparation, we stabilize the idler frequency to better than 1 MHz by locking it to a Doppler-free Lamb-dip detected in a room temperature gas cell filled with $\approx 50\text{ }\mu\text{bar}$ of methane. The homogenous linewidth of the ro-vibrational transitions in the molecular beam is typically 1–3 MHz due to the transit time broadening caused by the passage of the molecular beam through the focused IR beam.

For optical pumping by rapid adiabatic passage,²⁵ the OPO idler IR beam with a diameter of 3.8 mm (full width at $1/e$ of power profile on the lens) is focused by a $f = +25.4$ cm

cylindrical lens, located 34 cm from the molecular beam. The cylindrically focused IR beam crosses the molecular beam in the first or second differential pumping stage at a right angle.

Focusing the IR beam in the direction of the molecular beam propagation creates a wavefront curvature of the infrared beam. Passage of the molecular beam through the curved wavefronts generates a Doppler tuning effect producing a frequency chirp for the molecules passing through the IR beam with a maximum tuning rate of $v^2/(\lambda R(z))$,²⁵ where v is the beam velocity, λ the wavelength and $R(z)$ is the wavefront curvature at the crossing region. The waveform curvature at the laser/molecular beam intersection is controlled by the choice of focal length f for the cylindrical lens and the position of the lens from the molecular beam. With proper focusing and sufficient infrared power, complete population transfer is achieved by *rapid adiabatic passage* between the initial and final ro-vibrational levels that are connected by the IR field.²⁶ Without focusing, the population of the initial and final state connected by the coherent IR field will undergo Rabi-cycling while molecules are traversing the IR beam. The final population in the vibrationally excited state will be a sensitive function of the laser intensity, the transit time, and the transition dipole moment of the ro-vibrational transition. Creating an optical π -pulse (analogous to what is done with a radio frequency field in NMR to invert a 2-level system of nuclear spins) which would invert the populations of the ro-vibrational 2-level system is impossible to achieve here, because of the distribution of speeds in the molecular beam, the fact that transitions between different degenerate m-levels for a given J have different transition moments and different Rabi-frequencies and because of the variation of IR intensity for different parts of the molecular beam. At best one could saturate the 2-level system using Rabi cycling averaged over many cycles of the different Rabi frequencies and transfer 50% to the excited state, which can also be achieved by infrared pumping using incoherent light. On the other hand, excitation by RAP will invert a 2 level system independent of the precise conditions of laser intensity, molecular beam velocity, and Rabi frequency as long as some basic conditions are satisfied²⁵ and, therefore, provides a more robust excitation method that can be used to prepare pure beams of vibrationally excited states.

To detect the rovibrationally excited molecules prepared by IR-laser pumping, we use a room temperature pyroelectric detector, mounted on a linear motion feedthrough so that it can be inserted into the molecular beam in the third differential pumping stage. By chopping the excitation laser with an electromagnetic shutter at 2 Hz and lock-in detection of the pyroelectric detector signal, we can selectively monitor the flux of vibrationally excited molecules incident on the 2 mm diameter detector element. Figure 5 shows the measured laser power dependence of the pyroelectric signal for excitation of the antisymmetric C–H stretching ν_3 of CH_4 via the R(1) and R(0) ro-vibrational transitions ($\Delta J = +1$) in a beam of 100% CH_4 with a mean speed of 1000 m/s.

The measured bolometer signal is fitted by a function designed to model the power dependence of the excited fraction

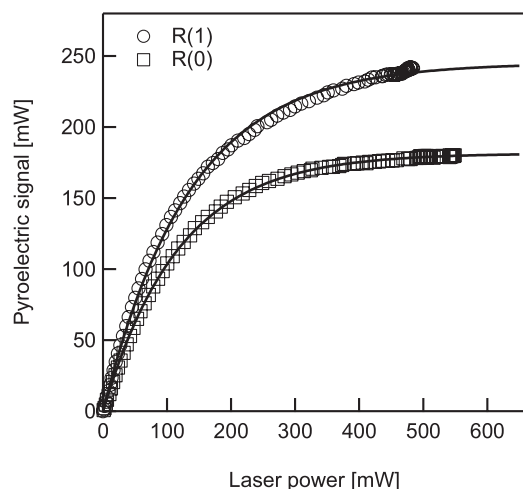


FIG. 5. Detection of vibrationally excited molecules in the molecular beam prepared by IR pumping and detected by a pyroelectric detector. The figure shows the laser power dependence of pyroelectric signal for excitation of $\text{CH}_4(\nu_3)$ originating from the $J = 0$ and $J = 1$ rotational states via the R(0) and R(1) transition.

prepared by IR pumping in the molecular beam.²⁷

$$y = A \{1 - \exp(-kP)\}. \quad (1)$$

Here, A and k are fitting parameters and P is the measured laser power used for IR pumping. The asymptote A corresponds to 100% population inversion between the initial rovibrational state $v = 0, J$ and the vibrationally excited state $\nu_3 = 1, J + 1$ by RAP as verified by a two-laser bleaching experiment which shows that the initial state can be completely depopulated by the RAP process. From the fits, we calculate the population transfer probability ($f_{p\text{-trans}}$) for R(1) and R(0) to be 98% and 99% at 500 mW of IR power, respectively. Moreover, the ratio between the asymptote value A for the R(1) and R(0) transitions reflects the relative population in the initial rotational states $J = 1$ and $J = 0$ which we use to estimate a rotational temperature (T_{rot}) of 25 K for the 100% CH_4 beam generated from a room temperature expansion nozzle. At $T_{\text{rot}} = 25$ K, the relative populations (f_p) in the initial rotational state $J = 0$ and $J = 1$ are 26% and 33% of the CH_4 in the beam, respectively. We then calculate the molecular beam excitation fraction as $f_{\text{exc}} = f_p \times f_{p\text{-trans}}$ to obtain 26% for IR pumping via R(0) and 32% for R(1) excitation.

C. Reflection absorption infrared spectroscopy

Our experiments make use of adsorbate detection by reflection absorption infrared spectroscopy to detect and quantify the formation of reaction products on the sample surface exposed to a molecular beam of state-prepared reactants. RAIRS is a surface sensitive vibrational spectroscopy technique that provides structure information about the adsorbed species on a reflective metal surface.^{18–20,28}

According to the surface selection rule,¹⁹ RAIRS detects molecular vibrations which have a component of their transition dipole moment directed along the surface normal. Vibrations for which the transition dipole moment lies in the plane of the surface cannot be detected by RAIRS. For max-

imum RAIRS detection sensitivity, we use a near grazing angle of incidence ($80^\circ \pm 5^\circ$) for the IR beam from the globar source of the FTIR spectrometer. Since only light with p-polarized light is absorbed by the adsorbates, we use a holographic wire-grid polarizer to linearly polarize the incident IR beam in the plane of incidence. With a cryogenically cooled InSb detector, we observe a peak-to-peak noise level of 1.5×10^{-5} absorption units when averaging 256 interferograms for a total acquisition time of 35 s. This translates to a detection sensitivity ($S/N = 1$) of 10^{-4} monolayer (ML) coverage of CO on Pt(111) or 1% ML $\text{CH}_3(\text{ads})$ absorbed on Pt(111) for 35 s acquisition time. The reason for the higher sensitivity for CO is the much larger transition dipole moment of the CO stretch vibration at 2085 cm^{-1} compared to that of the symmetric C–H stretch of $\text{CH}_3(\text{ads})$ at 2881 cm^{-1} .

1. Time-sequenced RAIRS data acquisition

After cleaning of the Pt(111) surface by Ar^+ ion sputtering followed by annealing and before each molecular beam deposition experiment, we record and average typically 1024 interferograms at 4 cm^{-1} resolution in 140 s to generate a single beam background spectrum of the clean surface. We then start to record a time sequence of sample interferograms averaging typically 512 scans and calculate a new single beam sample spectrum every 70 s. The ratio of the single beam sample spectrum and initially recorded single beam background spectrum contains information on any changes in absorption signal due to adsorption or desorption of surface species between the acquisition of the sample and background single beam spectra. We commence the molecular beam deposition after the first few sample spectra have been recorded to detect any possible adsorption from the UHV background. At a defined time $t_{\text{dep}} = 0$, a valve is opened to admit the molecular beam into the UHV chamber and expose the Pt(111) sample surface to the incident reactant molecules at normal incidence while continuing the acquisition of the sample interferograms.

Figure 6(a) shows an example of the time-evolution of the observed RAIRS spectra with increasing deposition time for a 3% CH_4/He molecular beam ($E_t = 47.7 \text{ kJ/mol}$, $T_n = 700 \text{ K}$) incident on a Pt(111) at a surface temperature $T_s = 150 \text{ K}$ for a deposition time of up to 80 min. Figure 6(b) shows the final RAIRS spectrum after 80 min deposition where the only detected product is $\text{CH}_3(\text{ads})$, characterized by a peak at 2881 cm^{-1} due to the symmetric C–H stretch and a weaker absorption signal at 2755 cm^{-1} due to a Fermi resonance between the bend overtone and the symmetric C–H stretch, in agreement with previous RAIRS studies of chemisorbed CH_3 on Pt(111).^{29,30}

2. RAIRS signal calibration and uptake curve

We calibrate the peak absorption signal for the RAIRS signal at 2881 cm^{-1} in terms of coverage $\theta(\text{CH}_3)$ using AES detection of the carbon coverage on Pt(111) due to the adsorption of CH_3 . In turn, the peak-to-peak AES signal ratio $C(272\text{eV})/\text{Pt}(237\text{eV})$ of the first derivative AES spectra was calibrated using the known saturation coverage for the

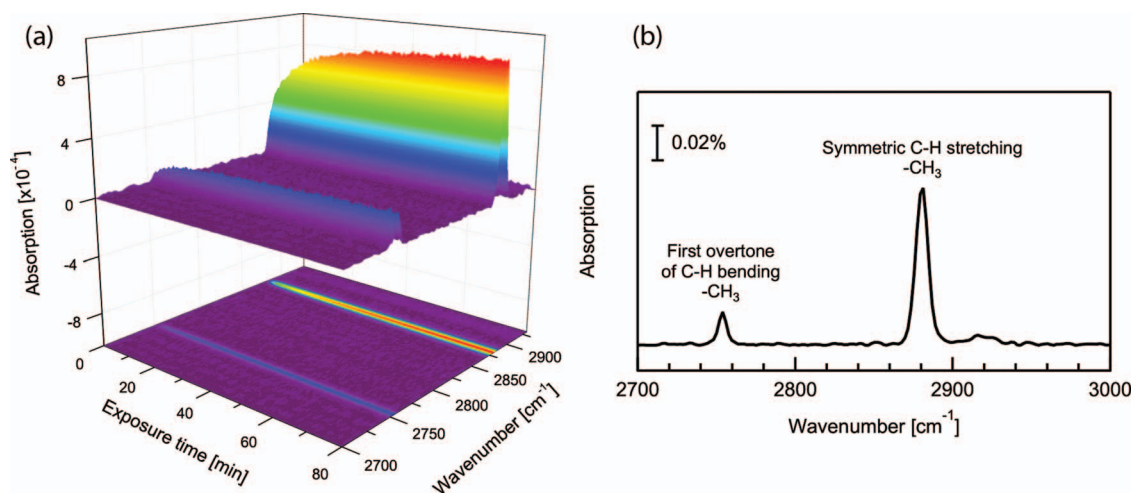


FIG. 6. RAIRS analysis of the $\text{CH}_3(\text{ads})$ uptake on Pt(111) at $T_s = 150$ K for an incident molecular beam of 3% CH_4 in ($E_t = 47.7$ kJ/mol, $T_n = 700$ K): (a) Time evolution RAIRS signals during 80 min molecular beam deposition and (b) final RAIR spectrum after 80 min deposition.

molecular adsorption of C_2H_4 on Pt(111) at $T_s = 140$ K of 0.25 ML (on Pt(111) $1\text{ML} = 1.51 \times 10^{15}$ atoms/cm 2).³¹

For the calibration of the RAIRS absorption signal and to verify its linearity with coverage, we measured both the RAIRS spectra and the carbon Auger signal for several different $\text{CH}_3(\text{ads})$ coverages produced by different exposure times of a clean Pt(111) surface to a 3% CH_4/He molecular beam. Figure 7 shows a graph of $\theta(\text{CH}_3)$ determined from the calibrated AES signal versus the CH_3 RAIRS peak absorption signal at 2881 cm^{-1} . The data points fall on a straight line indicating that the RAIRS absorption signal is, in fact, proportional to $\theta(\text{CH}_3)$, at least for $\theta(\text{CH}_3) < 0.25$ ML. The linear dependence of the $\text{CH}_3(\text{ads})$ RAIRS signal on coverage indicates negligible interactions between neighboring adsorbed CH_3 species consistent with the small transition dipole mo-

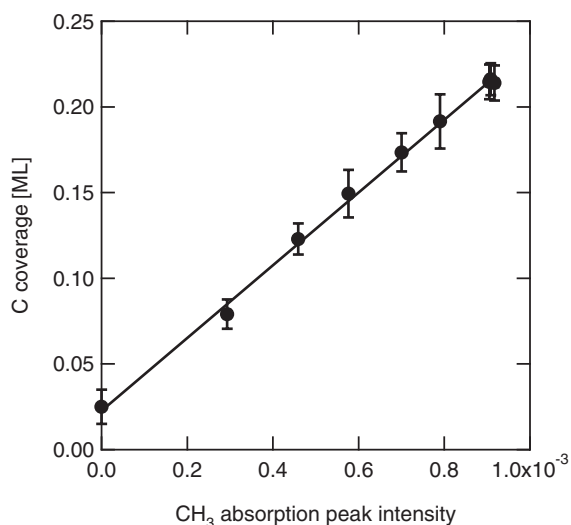


FIG. 7. Calibration of the RAIRS absorption signal $\text{CH}_3(\text{ads})$ at 2881 cm^{-1} in terms of C coverage on Pt(111) as determined by AES detection. The calibration data indicate a linear relationship between RAIRS absorption signal and $\text{CH}_3(\text{ads})$ coverage with a conversion of $\theta(\text{CH}_3)$ [ML] = 211 [ML/abs] · RAIRS + 0.025 .

ment of the symmetric CH_3 stretch. For absorbate vibrations with a stronger transition dipole such as the C–O stretch at 2085 cm^{-1} of chemisorbed CO on Pt(111) the RAIRS absorption signal shows a nonlinear dependence on coverage due to dipole-dipole interactions within the adsorbed layer of CO.³² The RAIRS calibration factor for the CH_3 RAIRS absorption signal at 2881 cm^{-1} in terms of coverage is obtained from the slope of the straight line fit $B = 211 \pm 11$ ML/absorption unit and the A intercept is due to a small carbon contamination of the cold Pt(111) surface during the Auger analysis.

With the known calibration factor, we convert the peak absorption signal at 2881 cm^{-1} measured by the RAIRS spectra to obtain the time dependent CH_3 coverage $\theta(\text{CH}_3)$ on Pt(111). To obtain the methyl uptake curve, i.e., $\theta(\text{CH}_3)$ as a function of incident methane dose, we monitor the methane flux (molecules/s) in the molecular beam using a calibrated mass spectrometer. The incident dose (units CH_4/cm^2 or ML where $1\text{ML} = 1.51 \times 10^{15}$ CH_4/cm^2 on Pt(111)) of methane is then calculated from the incident molecular beam flux and the molecular beam diameter on the target surface measured to be 7 mm by AES detection of C.

Figure 8(a) shows an example of an uptake curve for $\text{CH}_3(\text{ads})$ on Pt(111) at $T_s = 150$ K for a beam of incident CH_4 with kinetic energy of 75 kJ/mol at normal incidence. We parameterize the uptake curve by fitting a site-blocking Langmuir uptake model proposed by Killelea and co-workers³³ to the measured data points:

$$\theta_{\text{CH}_3}(D) = A \cdot \frac{B \cdot D}{1 + B \cdot D}. \quad (2)$$

The fitting parameters are the asymptotic saturation coverage A and the constant B . D is the molecular beam dose in ML units. The coverage dependent sticking probability $S(\theta)$ is given by the slope of the uptake curve, i.e., the derivative of Eq. (2) with respect to D with the S_0 , initial sticking probability as the initial slope of the uptake curve $S_0 = A \cdot B$.

Figure 8 compares measurements of the coverage dependent reaction probability by RAIRS (Fig. 8(a)) with simultaneous measurements in the same UHV chamber performed

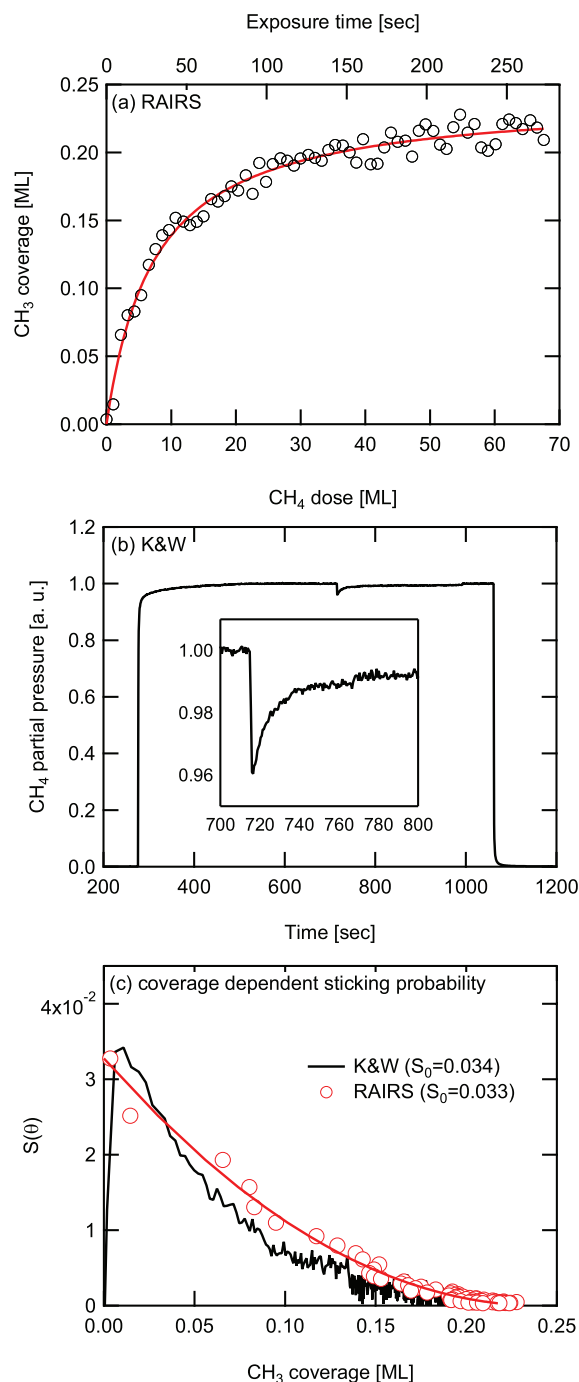


FIG. 8. (a) RAIRS measurement of methyl uptake from a $\sim 3\%$ CH₄/He ($T_n = 900$ K) molecular beam incident on Pt(111) at a surface temperature of 150 K; the solid line shows the fit of a site-blocking Langmuir uptake model (see text) to the data points to extract the coverage dependent sticking probability $S(\theta)$ from the slope of the uptake curve; (b) simultaneous measurement of $S(\theta)$ by the King & Wells (K&W) method (a); and (c) comparison of $S(\theta)$ measured by RAIRS (a) and K&W (b).

by the K&W method²² (Fig. 8(b)). For the analysis of K&W measurement, the time-dependent reaction probability is calculated as $S(t) = \Delta P(t)/\Delta P_0$, where ΔP_0 is the CH₄ partial pressure rise in the UHV chamber when the molecular beam is introduced and $\Delta P(t)$ is the time-dependent partial pressure drop due to CH₄ adsorption on the surface.

Figure 8(c) compares the $S(\theta)$ data obtained from RAIRS and K&W measurements. The results agree well if one takes into account the slower response times for the RAIRS measurement compared to the K&W detection (4.2 s versus 0.5 s). In principle, we could increase the time resolution of the RAIRS measurement by averaging fewer FTIR scans to minimize the averaging effect on S_0 but at the cost of lower S/N. The discrepancy between S_0 measured by K&W ($S_0 = 0.034 \pm 0.003$) and RAIRS ($S_0 = 0.033 \pm 0.004$) is within the error bars. The good agreement between the two independent methods validates our data analysis and the sticking probability data extracted from our RAIRS measurements. One important advantage of RAIRS is that it can measure lower sticking probabilities where $S_0 < 0.01\%$ beyond the 0.3% detection limit of the K&W measurements.

III. APPLICATION TO THE DISSOCIATIVE CHEMISORPTION OF METHANE ON Pt(111)

Figure 9 shows the RAIRS spectra of the nascent chemisorption products of five different methane isotopologues: CH₄, CH₃D, CH₂D₂, CHD₃, and CD₄ on Pt(111) formed at a surface temperature $T_s = 150$ K. Each spectrum was taken following an 80 min exposure of a clean Pt(111) to a molecular beam of the indicated methane isotopologues seeded in Helium (2%–4%) at $T_n = 700$ K. Due to the elevated nozzle temperature used and the inefficiency of vibrational cooling in a supersonic expansion, the methane dissociation is activated by a combination of incident translational energy ($E_t = 50$ –55 kJ/mol) and thermal vibrational excitation inside the 700 K nozzle ($E_{\text{vib}} = 5$ –10 kJ/mol). The five spectra enable us to assign the RAIRS signals for both the C–H and C–D cleavage products for each of the five methane isotopologues used as reactants. The ability of RAIRS to

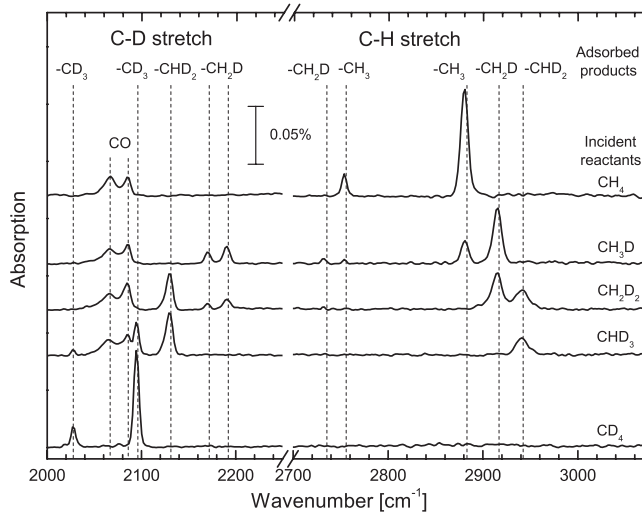


FIG. 9. RAIR spectra of the nascent chemisorption products for the five different methane isotopologues dissociating on Pt(111) at $T_s = 150$ K, activated by ~ 50 kJ/mol incident translational energy and 5–10 kJ/mol of thermal vibrational excitation from nozzle heating to 700 K. Both C–H and C–D cleavage products are observed for all partially deuterated methane isotopologues. Signals near 2060 cm⁻¹ (defect sites) and 2080 cm⁻¹ (terrace site) are due to a small coverage ($\leq 0.3\%$ ML) of a CO impurity in the molecular beam.

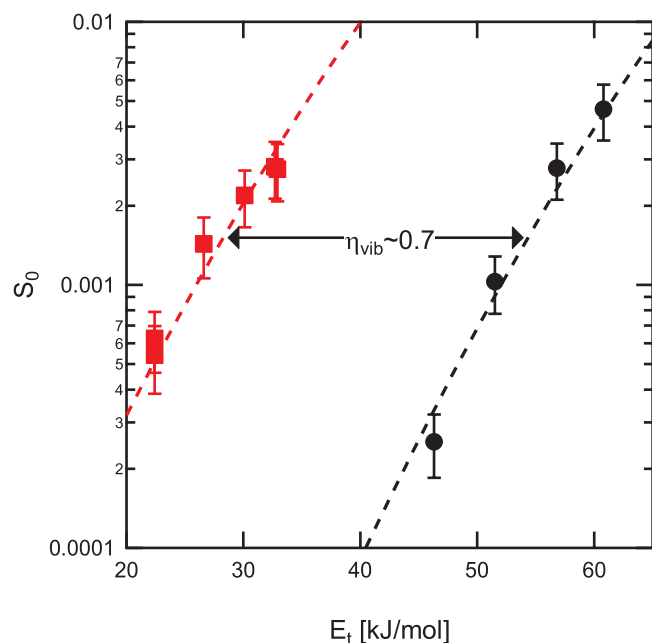


FIG. 10. Initial reactivity S_0 for (laser-off \bullet) and (ν_3 state-specific \blacksquare) as a function of normal incident translational energy E_t for dissociative chemisorption of CH_4 on Pt(111) at 150 K. The vibrational efficacy $\eta(\nu_3) \approx 0.7$ is given by the offset between the state-resolved sticking curves (dashed lines) and the vibrational energy of the ν_3 state. Error bars ($\sim 23\%$) are estimated from the relative errors in the coverage measurements (10%) and in the molecular beam flux measurements (13%).

distinguish different methyl species enables us to probe for vibrational bond-selectivity in the dissociative chemisorption of the three partially deuterated methane isotopologues on Pt(111).⁹

Figure 10 shows both the laser-off reaction probability $S_0(\text{laser-off})$ which represents an upper limit for the ground state ($\nu = 0$) reactivity, as well as the state-resolved reactivity $S_0(\nu_3)$ for CH_4 dissociation on Pt(111) at 150 K as a function of incident translational energy E_t obtained from the RAIRS measurements. The state-resolved reactivity measurements show that vibrational excitation of the incident CH_4 with one ν_3 -quantum of the anti-symmetric C–H stretch fundamental (3019 cm^{-1} of vibrational energy) enhances the CH_4 reactivity by more than a factor of 100 compared to the vibrational ground state ($\nu = 0$) for an incident translational energy $E_t = 34\text{ kJ/mol}$.

The effect of incident translational energy and state-specific vibrational energy of the prepared state ν on the dissociation probability of CH_4 is given by the vibrational efficacy $\eta(\nu)$ defined as

$$\eta(\nu) = \frac{E_0(\nu) - E_0(\nu = 0)}{h\nu}, \quad (3)$$

where $E_0(\nu)$ and $E_0(\nu = 0)$ are the average barrier heights for CH_4 dissociation in the vibrational state ν and $\nu = 0$, respectively. The change in average barrier height is determined by fitting so-called S-shaped reactivity curves³⁴ to the experimental reactivity data as shown by the dashed lines in Figure 10. The horizontal offset between the $\nu_3 = 1$ and the $\nu = 0$ curve represents the amount of incident translational

energy which results in the same increase in reactivity as one quantum of ν_3 vibration. A value of 0.7 for the ν_3 efficacy indicated that ν_3 vibrational energy is only 70% as efficient in activating the dissociation on Pt(111) as the same amount of incident energy in translation along the surface normal.

IV. SUMMARY

We describe a new molecular-beam/surface-science apparatus, which combines quantum state-specific preparation of gas-phase reactants by rapid adiabatic passage with RAIRS detection of surface products for state-resolved gas/surface reaction dynamics studies. The applications to methane chemisorption on Pt(111) presented here demonstrate that RAIRS is a powerful detection tool for highly detailed studies of surface reaction dynamics. Future applications will explore other vibrational states of methane including overtone and combination band prepared by double resonance excitation as well as other molecule/surface systems.

ACKNOWLEDGMENTS

We gratefully acknowledge the financial support provided by the Swiss National Science Foundation (Grant No. 134709/1) and the Ecole Polytechnique Fédérale de Lausanne.

- ¹I. Chorkendorff and J. W. Niemantsverdriet, *Concepts of Modern Catalysis and Kinetics*, 2nd ed. (Wiley-VCH, Weinheim, 2007).
- ²A. L. Utz, *Curr. Opin. Solid State Mater. Sci.* **13**(1–2), 4–12 (2009).
- ³L. B. F. Juurlink, D. R. Killelea, and A. L. Utz, *Prog. Surf. Sci.* **84**(3–4), 69–134 (2009).
- ⁴R. D. Beck and A. L. Utz, in *Dynamics of Gas-Surface Interactions: Atomic-Level Understanding of Scattering Processes at Surfaces*, edited by R. Díez Muiño and H. F. Busnengo (Springer, 2013).
- ⁵R. D. Beck, P. Maroni, D. C. Papageorgopoulos, T. T. Dang, M. P. Schmid, and T. R. Rizzo, *Science* **302**(5642), 98–100 (2003).
- ⁶P. Maroni, D. C. Papageorgopoulos, M. Sacchi, T. T. Dang, R. D. Beck, and T. R. Rizzo, *Phys. Rev. Lett.* **94**(24), 246104 (2005).
- ⁷R. Bisson, M. Sacchi, and R. D. Beck, *Phys. Rev. B* **82**(12), 121404(R) (2010).
- ⁸D. R. Killelea, V. L. Campbell, N. S. Shuman, and A. L. Utz, *Science* **319**(5864), 790–793 (2008).
- ⁹L. Chen, H. Ueta, R. Bisson, and R. D. Beck, *Faraday Discuss.* **157**, 285–295 (2012).
- ¹⁰B. L. Yoder, R. Bisson, and R. D. Beck, *Science* **329**(5991), 553–556 (2010).
- ¹¹K. G. Prasanna, R. A. Olsen, A. Valdes, and G. J. Kroes, *Phys. Chem. Chem. Phys.* **12**(27), 7654–7661 (2010).
- ¹²B. Jackson and S. Nave, *J. Chem. Phys.* **135**(11), 114701 (2011).
- ¹³M. P. Schmid, P. Maroni, R. D. Beck, and T. R. Rizzo, *Rev. Sci. Instrum.* **74**(9), 4110–4120 (2003).
- ¹⁴P. Maroni, D. Papageorgopoulos, A. Ruf, R. D. Beck, and T. R. Rizzo, *Rev. Sci. Instrum.* **77**(5), 054103 (2006).
- ¹⁵M. P. Schmid, P. Maroni, R. D. Beck, and T. R. Rizzo, *J. Chem. Phys.* **117**(19), 8603–8606 (2002).
- ¹⁶L. B. F. Juurlink, P. R. McCabe, R. R. Smith, C. L. DiCologero, and A. L. Utz, *Phys. Rev. Lett.* **83**(4), 868–871 (1999).
- ¹⁷R. Bisson, T. T. Dang, M. Sacchi, and R. D. Beck, *J. Chem. Phys.* **129**(8), 081103 (2008).
- ¹⁸M. Trenary, *Annu. Rev. Phys. Chem.* **51**, 381–403 (2000).
- ¹⁹F. M. Hoffmann, *Surf. Sci. Rep.* **3**(2–3), 107 (1983).
- ²⁰Y. J. Chabal, *Surf. Sci. Rep.* **8**(5–7), 211–357 (1988).
- ²¹S. L. Tang, J. D. Beckerle, M. B. Lee, and S. T. Ceyer, *J. Chem. Phys.* **84**(11), 6488–6506 (1986).

- ²²D. A. King and M. G. Wells, *Proc. R. Soc. London, Ser. A* **339**(1617), 245–269 (1974).
- ²³P. M. Hundt, R. Bisson, and R. D. Beck, *J. Chem. Phys.* **137**(7), 074701 (2012).
- ²⁴J. T. Yates, *Experimental Innovations in Surface Science: A Guide to Practical Laboratory Methods and Instruments* (Springer, New York, 1998).
- ²⁵N. V. Vitanov, T. Halfmann, B. W. Shore, and K. Bergmann, *Annu. Rev. Phys. Chem.* **52**, 763–809 (2001).
- ²⁶C. Liedenbaum, S. Stolte, and J. Reuss, *Phys. Rep.* **178**(1), 1–24 (1989).
- ²⁷P. R. McCabe, L. B. F. Juurlink, and A. L. Utz, *Rev. Sci. Instrum.* **71**(1), 42–53 (2000).
- ²⁸P. R. Griffiths and J. A. De Haseth, *Fourier Transform Infrared Spectrometry*, 2nd ed. (Wiley-Interscience, Hoboken, 2007).
- ²⁹I. J. Malik, M. E. Brubaker, S. B. Mohsin, and M. Trenary, *J. Chem. Phys.* **87**(9), 5554–5561 (1987).
- ³⁰D. J. Oakes, M. R. S. Mccoustra, and M. A. Chesters, *Faraday Discuss.* **96**, 325–336 (1993).
- ³¹K. Griffiths, W. N. Lennard, M. Iv, P. R. Norton, G. Pirug and H. P. Bonzel, *Surf. Sci.* **284**(1–2), L389–L393 (1993).
- ³²B. E. Heyden and A. M. Bradshaw, *Surf. Sci.* **125**(3), 787–802 (1983).
- ³³D. R. Killelea, V. L. Campbell, N. S. Shuman, R. R. Smith, and A. L. Utz, *J. Phys. Chem. C* **113**(48), 20618–20622 (2009).
- ³⁴A. C. Luntz, *J. Chem. Phys.* **113**(16), 6901–6905 (2000).